Original Article

# Imaging in detecting sites of pulmonary fibrosis induced by paraquat

**Xiao-li Xu, Wei Wang, Zu-jun Song, Hong Ding, Xiao-hong Duan, Huan-cheng Meng, Jian Chong**

*The Medical Team in Command Academy of the Frontier Control,Urumqi 830049,China (Xu XL); Emergency Medicine Department, Xijing Hospital, Fourth Military Medical University, Xi'an 710032, China (Wang W, Meng HC); Emergency Medicine Department, 309 Hospital of the People's Liberation Army, Beijing 100091, China (Song ZJ, Ding H); School of Stomatology, Fourth Military Medical University, Xi'an 710032, China (Duan XH, Chong J)*

***Corresponding Author:*** *Zu-jun Song, Email: songzj@fmmu.edu.cn*

**BACKGROUND:** The most common cause of death from paraquat (PQ) poisoning is respiratory failure from pulmonary fibrosis, which develops through pathological overproduction of extracellular matrix proteins such as collagens. In this study, a MicroCT system was used to observe dynamic changes of pulmonary fibrosis in rats with PQ poisoning, and find the characteristics of interstitial lung diseases via density-based and texture-based analysis of CT images of the lung structure.

**METHODS:** A total of 15 male SD rats were randomly divided into a control group ($n$=5) and a PQ poisoning group ($n$=10). The rats in the poisoning group were intraperitoneally administered with 4 mg/ mL PQ at 14 mg/kg, and the rats in the control group were administered with the same volume of saline. The signs of pulmonary fibrosis observed by the MicroCT included ground-glass opacity, nodular pattern, subpleural interstitial thickening, consolidation honeycomb-like shadow of the lung.

**RESULTS:** Compared with the control group, the rats with acute PQ poisoning had different signs of pulmonary fibrosis. Ground-glass opacity and consolidation of the lung appeared at the early phase of pulmonary fibrosis, and subpleural interstitial thickening and honeycomb-like shadow developed at the middle or later stage. MicroCT images showed that fibrotic lung tissues were denser than normal lungs, and their density was up-regulated with pulmonary fibrosis. There was no difference in the progress of pulmonary fibrosis between the right lung and the left lung ($P$>0.05), but there were differences in fibrosis degree at different sites in the lung ($P$<0.05 or $P$<0.01). Pulmonary fibrosis was mainly seen in the exterior area of the middle-lower part of the lung.

**CONCLUSION:** Imaging can show the development of pulmonary fibrosis in PQ poisoning rats, and this method may help to administer drugs more reasonably in treating pulmonary fibrosis.

**KEY WORDS:** MicroCT; CT value; Paraquat; Pulmonary fibrosis; Region of interest

*World J Emerg Med 2011;2(1):45-49*

## INTRODUCTION

As an effective organic heterocyclic herbicide, 1,1'-Dimethyl-4,4'-bipyridinium dichloride (paraquat, PQ) is also a lethal poison. In some developing countries, where paraquat is cheap and easily accessible, many people have taken it for suicide. PQ poisoning remains a global health problem. Despite studies and clinical practice in the last few decades, little improvement has been made in reducing the fatality of PQ poisoning , but there is a comparatively high mortality of patients with PQ poisoning.

The lung is the main target organ of PQ poisoning. PQ mainly accumulates in the lung (pulmonary concentrations can be 6 to 10 times higher than those in the plasma), where it is retained even when the blood concentration decreases. The most common cause of death from PQ poisoning is respiratory failure from pulmonary fibrosis, which develops through pathological overproduction of extracellular matrix proteins such as collagens.[1] In this study, we used a micro-computed tomography (MicroCT) system to observe the dynamic changes of pulmonary fibrosis in PQ poisoning rats *in vivo*, and find the characterization of interstitial lung diseases via density-based and texture-based analysis of CT images of lung structure and function.[2]

 

# METHODS

## Animals and instruments

Fifteen clean male Sprague-Dawley rats, weighing 204±10 g, were purchased from the Experimental Animal Center of the Fourth Military Medical University, and the certificate number was SCXK (Army) 2002-2005. The paraquat solution was purchased from Eastern Sichuan Chemical Co., Ltd. (Sichuan, China), and its active ingredient content was 200 g/L, with a production license XK 13-003-00058. Sodium pentobarbital was purchased from Shanghai Experiment Reagent Co., Ltd., China Medicine Group (Shanghai, China), and the MicroCT system was from Siemens (Munich, Germany).

## Animal model of pulmonary fibrosis

This study was approved by the Committee of Laboratory Animal Care of the Fourth Military Medical Univeisity. One mL paraquat solution (concentration 20%) was diluted into 50 mL solution by mixing with sterile isotonic saline at a concentration of 4 mg/mL. The SD rats were intraperitoneally administered with 4 mg/mL PQ at 8, 10, 12, 14, 16, 18, 20 mg/ kg respectively to establish models of pulmonary fibrosis. The models were used to study the pharmacodynamics of PQ and observe the changes of lung injury at 4 weeks after injection. PQ injected intraperitoneally at 14 mg/kg showed the best result.

Fifty male SD rats were randomly divided into a control group ($n$=5) and a PQ poisoning group ($n$=10). The rats in the posioning group were intraperitoneally administered with 4 mg/mL PQ at 14 mg/kg, and the rats in the control group were administered with the same volume of saline. The rats were fed in an environment with a temperature of 24±2 °C and a humidity of 60%±5%, where adequate food and water were provided and the stool of the rats was timely removed.

## Parameters

### *Detection method*

At 3, 7, 14, 28 days after injection of PQ, all rats were anesthetized intraperitoneally with 1% sodium pentobarbital at a dose of 40 mg/kg. The anesthetized rats were placed and fixed on the scanning table, and the MicroCT system was used to scan the lungs. The parameters of scanning were as follows: voltage 80 kVp and current 500 μA for a tube, exposure time 1000ms, scan mode 360°, incremental angle 1.0°; detector assembly mode 4×4; average frame 2, and scanning time about 12 minutes.

### *Observed parameters and division of region of interest (ROI)*

The pulmonary fibrosis signs observed by the MicroCT included ground-glass opacity, nodular pattern, subpleural interstitial thickening, consolidation honeycomb-like shadow of the lung. ROI was defined as follows; the general location of horizontal crack and oblique crack of the right lung; both lungs divided into upper, middle, and lower parts on the coronal images of the lung and five zones with the same area which were drawn in each part of the lung and served as a determination area (Figure 1A); ten zones with the same area which were drawn in each lung and served as a determination area (Figure 1B).

### *Image evaluation*

After the lung tissue was scanned by the Micro CT, the workstation automatically generated image, post-processing process was performed by installed software, and CT value was recorded. The differences of pulmonary fibrosis signs were compared between the four time points in the poisoning group, and between the poisoning group and the control group. The image was evaluated by two experienced radiologists.

## Statistical analysis

All data were expressed as percentage or mean ± standard deviation, unless indicated. When the two groups (the upper and lower parts of unilateral lung) were compared, Student's $t$ est was used for statistical analysis. Statistical

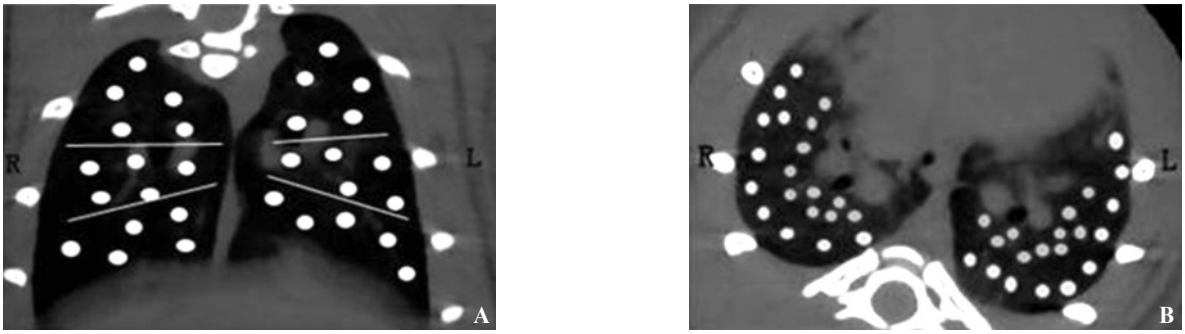


**Figure 1.** The division of ROI. A: five zones with the same area in each part of the lung and served as a determination area; B: ten zones with the same area in each lung and served as a determination area.

analysis were performed using the Statistical Package for the Social Sciences (SPSS) version 12.0 software. A *P* value less than 0.05 was considered to be statistically significant.

# RESULTS

## Pulmonary fibrosis signs

The images of pulmonary fibrosis signs are shown in Figure 2. The five above-mentioned pulmonary fibrosis signs appeared differently at four time points (Table 1). About 83.3% ground-glass opacity and 77.8% consolidation of the lung developed at 3 and 7 days after treatment, about 66.7% nodules developed at 7 days after treatment, about 66.7% subpleural interstitial thickening developed at 14 days after treatment, and all honeycomb-like shadow developed at 14 and 28 days after treatment (Table 1).

## CT values of ROI in coronal image

CT values of ROI in coronal image are shown in Table 2. These values were close to zero with the time; no difference was observed in the CT values of the same part between the left and right lungs ($P>0.05$). Three days after treatment, significant difference was seen between the middle , lower and upper parts ($P<0.05$), but no difference between the middle and lower parts in the same lung ($P>0.05$).

**Table 1.** The signs of pulmonary fibrosis at 3, 7, 14, 28 days after treatment (no.%)

| Time (days) | Opacities | Nodule | Thickening | Consolidation | Honeycomb |
|---|---|---|---|---|---|
| 3 | 3 (50) | 0 (0) | 0 (0) | 4 (44.4) | 0 (0) |
| 7 | 5 (83.3) | 2 (66.7) | 1 (33.3) | 7 (77.8) | 0 (0) |
| 14 | 6 (100) | 3 (100) | 3 (100) | 8 (88.9) | 1 (50) |
| 28 | 6 (100) | 3 (100) | 3 (100) | 9 (100) | 2 (100) |

## CT values of ROI in cross-sectional image

CT values of ROI in cross-sectional image are shown in Table 3. These values were close to zero with the time. Except in the peripheral part, no difference was seen in the CT values of the same part between the left and right lungs ($P>0.05$). Except 3 days after treatment, significance difference was found between the peripheral and central parts in the same lung ($P<0.01$).

# DISCUSSION

Cone-beam microCT is one of the most popular choices for small animal imaging which is an important tool for studying animal models with transplanted diseases. Region-of-interest (ROI) imaging techniques in CT, which reconstruct an ROI image from the projection data of ROI can be used not only for reducing imaging-radiation exposure to the subject and scatters to the detector but also for potentially increasing spatial

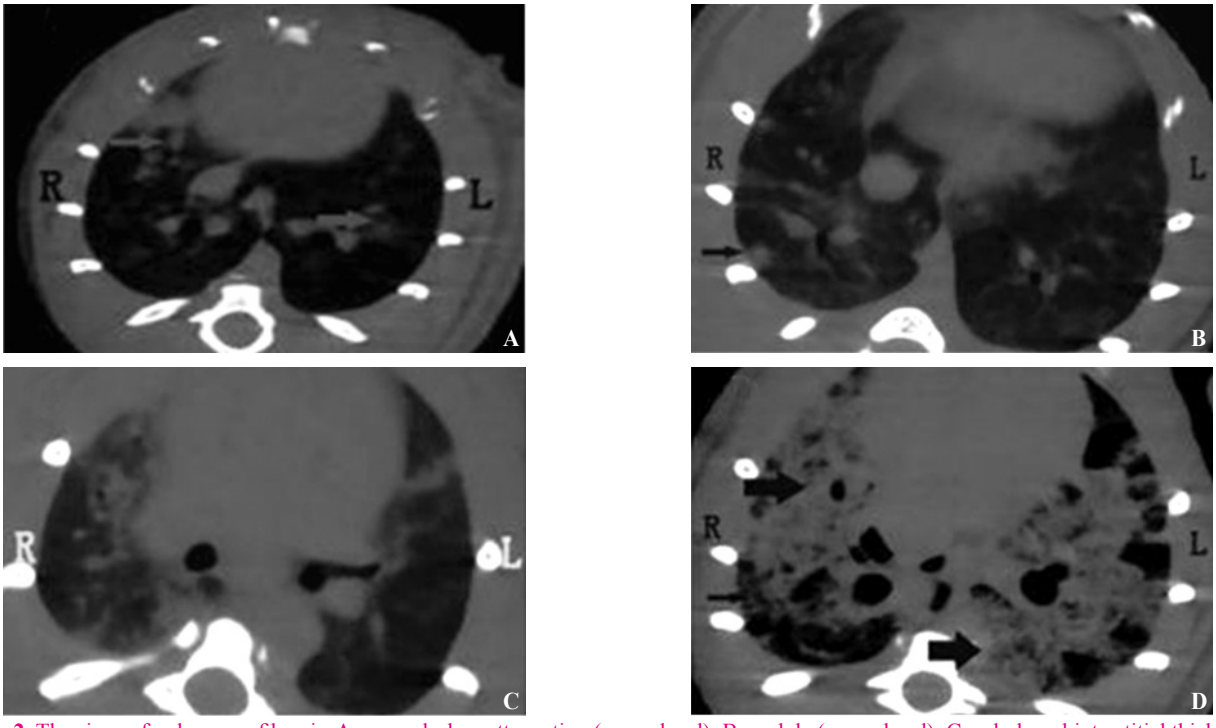


**Figure 2.** The signs of pulmonary fibrosis. A: ground-glass attenuation (arrow head); B: nodule (arrow head); C: subpleural interstitial thickening; D: consolidation (bold arrow) and honeycomb lung (slimsy arrow head).

**Table 2.** CT values of ROI in coronal image (mean±SD, negative values)

| Groups | *n* | Right lung | | | Left lung | | |
|---|---|---|---|---|---|---|---|
| | | upper | middle | lower | upper | middle | lower |
| Control | 25 | 708.93±19.55 | 712.51±32.97 | 712.69±23.24 | 716.64±24.58 | 712.28±20.95 | 714.55±24.92 |
| Poisoning (days) | | | | | | | |
| 3 | 50 | 616.14±7.99 | 614.48±10.24 | 614.30±9.43 | 615.21±9.22 | 615.75±9.29 | 612.39±9.58 |
| 7 | 50 | 521.33±12.05 | 515.52±13.60$^{\Delta}$ | 514.18±14.05$^{\blacktriangle}$ | 519.36±12.44 | 512.83±10.25$^{\Delta\Delta}$ | 512.01±11.91$^{\blacktriangle}$ |
| 14 | 50 | 325.99±10.04 | 317.88±9.29$^{\Delta\Delta}$ | 319.20±9.46$^{\blacktriangle}$ | 323.19±11.24 | 316.30±9.16$^{\Delta\Delta}$ | 317.48±8.15$^{\blacktriangle}$ |
| 28 | 50 | 198.82±5.82 | 189.91±4.97$^{\Delta\Delta}$ | 188.24±4.38$^{\blacktriangle}$ | 202.13±3.73 | 189.10±5.36$^{\Delta\Delta}$ | 186.73±4.32$^{\blacktriangle\bigstar}$ |

Compared between the upper and middle parts of the same lung, $^{\Delta}P<0.05$, $^{\Delta\Delta}P<0.01$; compared between the upper and lower parts of the same lung, $^{\blacktriangle}P<0.01$; compared between the middle and lower parts of the same lung, $^{\bigstar}P<0.05$.

**Table 3.** CT values of ROI in cross-sectional image (mean±SD, negative values)

| Groups | *n* | Right central part | Left central part | Right peripheral part | Left peripheral part |
|---|---|---|---|---|---|
| Control | 50 | 709.34±11.52 | 711.02±13.16 | 712.44±12.06 | 711.76±13.04 |
| Poisoning (days) | | | | | |
| 3 | 100 | 618.09±9.36 | 620.31±10.01 | 615.98±8.91 | 616.02±8.78$^{\blacktriangle}$ |
| 7 | 100 | 520.65±8.29 | 521.37±7.92 | 516.02±9.33$^{\blacktriangle}$ | 513.27±8.61$^{\Delta\blacktriangle}$ |
| 14 | 100 | 325.01±8.99 | 322.78±10.20 | 318.74±9.71$^{\blacktriangle}$ | 319.06±9.12$^{\blacktriangle}$ |
| 28 | 100 | 199.38±11.06 | 200.07±9.51 | 189.41±8.87$^{\blacktriangle}$ | 187.58±9.26$^{\blacktriangle}$ |

Compared between the right and left lungs, $^{\Delta}P<0.01$; compared between peripheral and central parts within the same lung, $^{\blacktriangle}P<0.01$.

resolution of the reconstructed images. Increasing spatial resolution in microCT images can facilitate improvement of accuracy in many assessment tasks.[3-5] MicroCT can be applied in scanning for minimally invasive, longitudinal observations of *in vivo* pathological changes associated with a variety of pulmonary disease models. It is suitable for repeated measurements of the same animal over time. This approach could be used to make baseline evaluation in each animal before fibrosis is induced. Then the fibrosis is confirmed before treatment and potential treatment effects are subsequently evaluated. The technique has replaced invasive histological evaluation.

Based on the X-ray attenuations obtained from different angles, a cross-sectional image of the body can be calculated.[6] Each pixel of the reconstructed image is defined as an X-ray attenuation value (also called a CT number) which is expressed in Hounsfield Units (HU). The Hounsfield scale is calibrated in a way that yields 0 HU for water and -1000 HU for air. CT numbers within one cross-section of the body can thus range from -1000 (e.g., the lungs) to several thousand HU (e.g., bone or metal).[7,8] MicroCT has become a useful tool to detect the relevant position of lesions by illustrating density contrast between the lesions and normal tissues nearby[8,9] and to assess the severity of the lesions. For example, pulmonary fibrosis can be quantified by detecting which part of the lung is out of the range of specific density or appropriate Hounsfield unit.[8,10]

Although the mortality of PQ poisoning has been improved, many patients die of progressive pulmonary fibrosis and respiratory failure.[11] Pulmonary fibrosis as a secondary effect of other diseases can be classified as interstitial lung diseases like autoimmune disorders, viral infections or microscopic injuries to the lung. Diseases and conditions that may cause pulmonary fibrosis as a secondary effect are as follows: (1) inhalation of environmental and occupational pollutants such as asbestosis, silicosis and exposure to certain gases in coal miners, ship workers and sand blasters. Hypersensitive pneumonitis resulting from inhaling dust contaminating with bacterial, fungal, or animal products; (2) cigarette smoking increasing the risk or making the illness worse; (3) some typical connective tissue diseases such as rheumatoid arthritis, SLE and scleroderma; (4) other diseases involving connective tissues such as sarcoidosisand Wegener's granulomatosis; (5) infections; (6) certain medications, e.g. amiodarone, bleomycin, busulfan, methotrexate, and nitrofurantoin; and (7) radiation therapy to the chest. In addition, the activation of fibroblasts increases proliferation and promotes fibroblast differentiation into collagen-producing myofibroblasts,[15] and the balance of collagen metabolism is destroyed. This also contributes to the development of pulmonary fibrosis.[16-22]

Our study showed the CT images of the rats with acute PQ poisoning had different signs of pulmonary fibrosis, more signs developed with the poisoning time, and mainly appeared at one week after treatment. In general, ground-glass opacity and consolidation of the lung appeared at the early phase of pulmonary fibrosis, and the subpleural interstitial thickening and honeycomb-like shadow developed at the middle or later stage.[23] In MicroCT images, fibrotic lung tissues were denser than normal lungs, and their density was up-regulated

by pulmonary fibrosis. Analysis of the CT data revealed that there was no difference in the progress of pulmonary fibrosis between the right and left lungs ($P>0.05$), but there were differences in fibrosis degree at different sites of the lung ($P<0.05$ or $P<0.01$). Pulmonary fibrosis is mainly distributed in the exterior area of the middle and lower parts of the lung.

In this study, imaging was used to observe the development of pulmonary fibrosis in PQ poisoning rats, and this method may be helpful to administrate drugs more reasonably in treating pulmonary fibrosis.

**Funding:** None.
**Ethical approval:** Not needed.
**Conflicts of interest:** No benefits in any form have been received or will be received from a commercial party related directly or indirectly to the subject of this article.
**Contributors:** Wang W drafted the paper. All authors read and approved the final version.

## REFERENCES

1 Hagiwara S, Iwasaka H, Matsumoto S, Noguchi T. An antisense oligonucleotide to HSP47 inhibits paraquat-induced pulmonary fibrosis in rats. Toxicology 2007; 236: 199-207.
2 Hoffman EA, Reinhardt JM, Sonka M, Simon BA, Guo J, Saba O, et al. Characterization of the interstitial lung diseases via density-based and texture-based analysis of computed tomography images of lung structure and function. Acad Radiol 2003; 10: 1104-1118.
3 Kinney JH, Lane NE, Haupt DL. In vivo, three-dimensional microscopy of trabecular bone. J Bone Miner Res 1995; 10: 264-270.
4 David W, Michael M. Micro-CT in small animal and specimen imaging. Trends Biotechnol 2002; 20: s34-s39.
5 Badea C, Hedlund LW, Johnson GA. Micro-CT with respiratory and cardiac gating. Med Phys 2004; 31: 3324-3329.
6 Schuster DP, Kovacs A, Garbow J, Piwnica-Worms D. Recent advances in imaging the lungs of intact small animals. Am J Respir Cell Mol Biol 2004; 30: 129-138.
7 Bushberg JT, Seibert JA, Leidholdt EM, Boone JM. Essential Physics of Medical Imaging. 2nd. Baltimore, MD: Lippincott Williams and Wilkins, 2001. ISBN: 9780683301182.
8 Kennita AJ. Imaging techniques for small animal imaging models of pulmonary disease: micro-CT. Toxicol Pathol 2007; 35: 59-64.
9 Walters EB, Panda K, Bankson JA, Brown E, Cody DD. Improved method of in vivo respiratory-gated micro-CT imaging. Phys Med Biol 2004; 49: 4163-4172.
10 Hoffman EA, Reinhardt JM, Sonka M, Simon BA, Guo J, Saba O, et al. Characterization of the interstitial lung diseases via density-based and texture-based analysis of computed tomography images of lung structure and function. Acad Radiol 2003; 10: 1104-1118.
11 Hong SY, Yang JO, Lee EY, Lee ZW. Effects of N-acety-L -cysteine and glutathione on antioxidant status of human serum and 3T3 fibroblasts. J Korea Med Sci 2003; 18: 649-654.
12 Nakamura T, Ushiyama C, Shimada N, Hayashi K, Ebihara I, Suzaki M, et al. Changes in concentrations of type IV collagen and tissue inhibitor of metalloproteinase-1 in patients with paraquat poisoning. J Appl Toxicol 2001; 21: 445-447.
13 Kuwano K, Hagimoto N, Kawasaki M, Yatomi T, Nakamura N, Nagata S, et al. Essential roles of the Fas-Fas ligand pathway in the development of pulmonary fibrosis. J Clin Invest 1999; 104: 13-19.
14 Zhang J, Lv G, Zhao Y. The significance of serum xanthine oxidase and oxidation markers in acute paraquat poisoning in humans. Clin Biochem. 2010 Sep 22. [Epub ahead of print]
15 Bogatkevich GS, Tourkina E, Silver RM, Ludwicka-Bradley A. Thrombin differentiates normal lung fibroblasts to a myofibroblast phenotype via the proteolytically activated receptor-1 and a protein kinase C-dependent pathway. J Biol Chem 2001; 276: 45184-45192.
16 Cook DN, Brass DM, Schwartz DA. A matrix for new ideas in pulmonary fibrosis. Am J Respir Cell Mol Biol 2002; 27: 122-124.
17 Janssen-Heininger YM, Poynter ME, Baeuerle PA. Recent advances towards understanding redox mechanisms in the activation of nuclear factor kappaB. Free Radic Biol Med 2000; 28: 1317-1327.
18 Yamashita M, Ando Y. A long-term follow-up of lung function in survivors of paraquat poisoning. Hum Exp Toxicol 2000; 19: 99-103.
19 Satomi Y, Tsuchiya W, Mihara K, Ota M, Kasahara Y, Akahori F. Gene expression analysis of the lung following paraquat administration in rats using DNA microarray. J Toxicol Sci 2004; 29: 91-l00.
20 Ho AK, McNeil L, Terriff D, Price DM, Chik CL. Role of protein turnover in the activation of p38 mitogen-activated protein kinase in rat pinealocytes. Biochem Pharmacol 2005; 70: 1840-1850.
21 Ruiz V, Ordóñez RM, Berumen J, Ramírez R, Uhal B, Becerril C, et al. Unbalanced collagenases / TIMP-1 expression and epithelial apoptosis in experimental Lung fibrosis. Am J Physiol Lung Cell Mol Physiol 2003; 285: 1026-1036.
22 Peter A, Gergely P. Metabolic switches of T-cell activation and apoptosis. Antioxidants Redox Signaling 2002; 4: 427-443.
23 Kaner RJ, Ladetto JV, Singh R, Fukuda N, Matthay MA, Crystal RG. Lung overexpression of the vascular endothelial growth factor gene induces pulmonary edema. Am J Respir Cell Mol Biol 2000; 22: 657-664.

*Received September 17, 2010*
*Accepted after revision February 16, 2011*